

SCIENTIFIC REPORTS



OPEN

Near-zero metamaterial inspired UHF antenna for nanosatellite communication system

Touhidul Alam¹, Mohammad Tariqul Islam^{1,2} & Mengu Cho^{2,3}

Epsilon-and-mu-near-zero (EMNZ) metamaterial structure inspired UHF antenna for nanosatellite has been proposed in this paper. The antenna consists of 3×2 -unit cell array on the ground plane and a meander line radiating patch. Coaxial probe feeding technique has been obtained to excite the antenna. The meander line enables the antenna to resonate at lower UHF band and the metamaterial array is used to make the resonant frequency stable by reducing the coupling effect with metallic nanosatellite structure. The metamaterial structure exhibits EMNZ characteristics from 385 MHz to 488.5 MHz, which facilitates stable resonant frequency and higher antenna efficiency when embedded with nanosatellite structure. The proposed EMNZ inspired antenna has achieved measured impedance bandwidth ($S_{11} < -10$ dB) of 14.92 MHz (391 MHz–405.92 MHz). The perceptible novelty of this paper is the development of EMNZ metamaterial that significantly improves the UHF antenna's operating frequency stability as well as efficiency for low earth orbit nanosatellite communications.

Over the last decade, nanosatellite missions have increased vividly for low earth orbit space missions. This concept has been very enthusiastic to the scientific, private, and government missions due to miniature electronics size with low-cost and low power consumption¹. Nanosatellite space missions are being fruitful in coastal and inland critical observation of natural disaster, monitoring agri-environmental and agriculture conditions, and space atmosphere observation. Every nanosatellite has some common functions for satellite operations like power system, uplink-downlink communications, and altitude control. The antenna is the key element of the uplink-downlink communications between satellite and Earth. The inherent relation between lower frequency and antenna size compels antenna researchers to compromise with antenna gain and efficiency for compliance with the CubeSat standards. So, antenna design for nanosatellites has been a critical issue to the CubeSats researchers, especially for lower frequency². Deployable wire antennas like monopoles dipoles, helical and Yagi-Uda arrays antennas are widely used in recent nanosatellite missions³. But mechanical deployment is quite sophisticated and this might increase the chance of mission failure⁴. Several nanosatellite missions have been failed due to antenna deployment complexity^{5–7}.

In contrast to the deployable antenna, patch antenna provides a low profile and improve the mission reliability; and makes the patch antennas are a good replacement of wire antennas. However, UHF patch antenna occupies large amount the nanosatellite body surface and introduce complexity to integrate sufficient solar cells. So, designing a small size ultra-high frequency (UHF) patch antenna strategically integrated with the satellite body and that do not require mechanical deployment has become a big challenge for nanosatellite and antenna researchers. Several research efforts have been devoted to designing a miniature UHF patch antenna with good impedance bandwidth, efficiency, and gain. Reactive impedance surface based U-slot patch antenna is one of them⁸, where the antenna achieved lower UHF band (410–485 MHz) with antenna size reduction. However, the area of the antenna is $220 \times 220 \times 20$ mm³ and the antenna is incompatible with CubeSat structure. In⁹, to reduce the conventional RIS antenna size two-layer mushroom-like RIS is presented for 400 MHz UHF wireless communication, where the size is $66 \times 66 \times 11.2$ mm³. Though the technique reduced the antenna size, antenna higher antenna height remains a critical issue for nanosatellite communication. Meander line technology facilitates

¹Centre of Advanced Electronic & Communication Engineering, Faculty of Engineering and Built Environment, Universiti Kebangsaan Malaysia, Bangi, Selangor D.E., 43600, Malaysia. ²Laboratory of Spacecraft Environment Interaction Engineering (LaSEINE), Kyushu Institute of Technology (Kyutech), Kitakyushu-shi, Fukuoka, Japan.

³School of Electrical and Electronic Engineering, Nanyang Technological University, Nanyang Drive, Nanyang, Singapore. Correspondence and requests for materials should be addressed to T.A. (email: touhid13@siswa.ukm.edu.my) or M.T.I. (email: tariqul@ukm.edu.my)

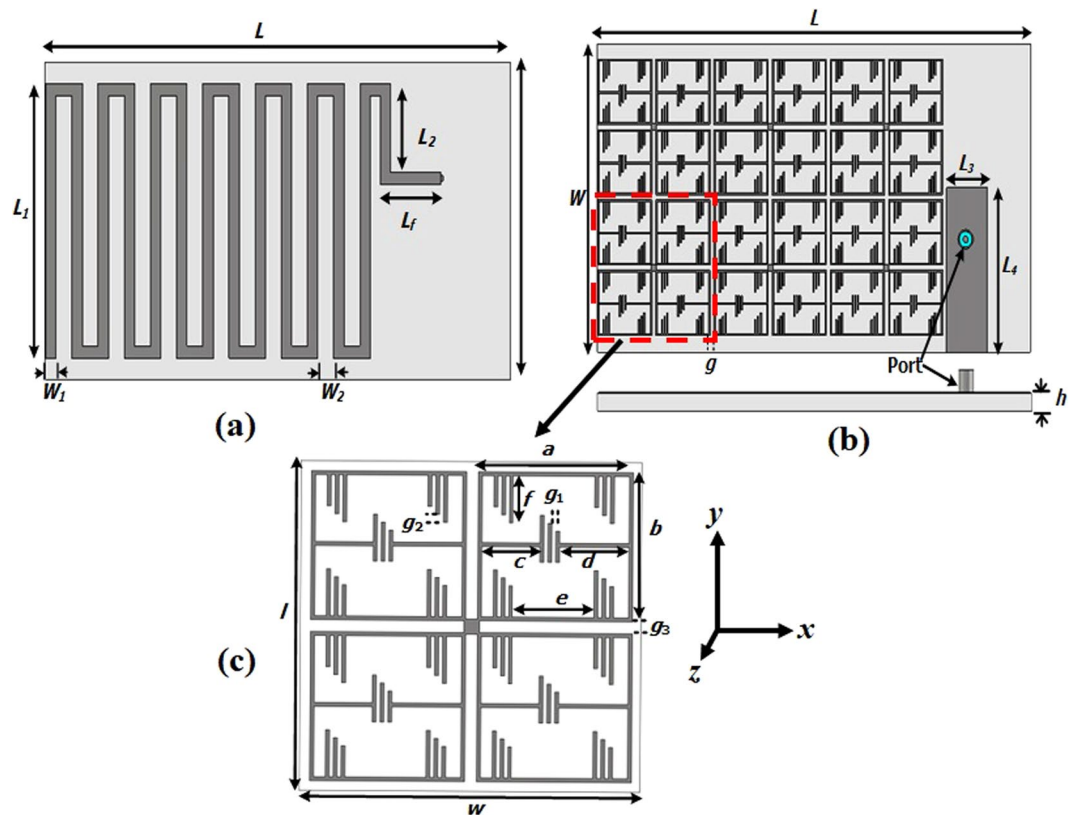


Figure 1. Proposed metamaterial antenna configuration (a) Top view, (b) bottom view and (c) metamaterial structure.

achievement of the lower band with small antenna size¹⁰. However, this type of antenna does not work effectively when embedded in the complex structure and would degrade its radiation efficiency. To overcome this problem, epsilon-and-mu-near-zero (EMNZ) metamaterial has been developed and included in the ground plane of the antenna.

There have been a lot of research efforts since the last decades in the field of artificially engineered materials that show infrequent properties and do not readily exist in nature^{11–14}. The unique properties metamaterial such as negative permittivity, permeability, refractive index or double negative characteristic have been utilized to improve antenna characteristics. Besides, metasurfaces structure, another form of engineered materials has been utilized to enhance antenna performance¹⁵, linear to circular polarization conversion¹⁶, and wavefronts control¹⁷, etc. Now, researchers show their interest in another type of engineered material known as near-zero-metamaterials. This is the type of metamaterials whose metamaterial characteristics are near to zero like epsilon-near-zero (ENZ), mu-near-zero (MNZ), or both epsilon-and-mu-near-zero (EMNZ)^{18,19}. Metamaterial with individual ENZ or MNZ shows impedances mismatch in the free space, which occurs high reflectance, high impedance and high loss²⁰. However, EMNZ has low loss since the impedance is matched with free space. This type of metamaterial has been efficiently used in the field of antenna and wave propagation for enhancing the radiation efficiency, antenna size miniaturizing, coupling effect reduction, or for modifying the radiation patterns^{20–23}.

In this paper, an EMNZ metamaterial inspired printed patch antenna is proposed for the lower UHF communication system. This antenna is inspired from a conventional meander line patch antenna with EMNZ metamaterial ground plane to improve efficiency and impedance matching over the desired frequency range. Moreover, a technique using metamaterial array elements reduce the EM coupling with nanosatellite structure of the conventional meander line antenna, while maintaining good impedance matching and efficiency for the UHF communication system. Moreover, the antenna is designed to fit into commercially available nanosatellite structures to mitigate antenna deployment complexity.

Antenna Design Methodology

The meander-line antenna concept is to fold the conductors back and forth to reduce antenna physical size. The resonant frequency of the conventional meander line antenna can be achieved by increasing the width of the meander line which leads the capacitance to the ground plane or increasing the meander line section to generate effective self-inductance for lower frequency adjustment. In this proposed design, the main parameters have been optimized by tuning line width, number of folds, the distance between folds to reduce the antenna size. As the physical dimension of the antenna is reduced, the antenna radiation efficiency and bandwidth are also decreased. To enhance radiation performance, EMNZ metamaterial structure has been used in the ground plane of the

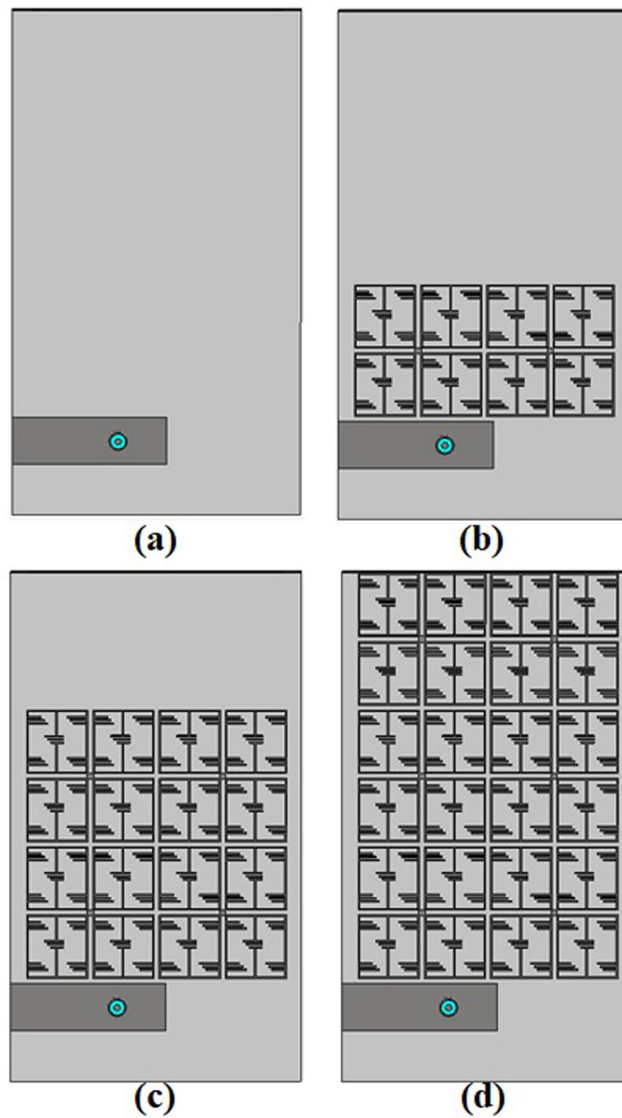


Figure 2. Design evolution of the proposed UHF antenna: (a) antenna 1, (b) antenna 2, (c) antenna 3 and (d) antenna 4.

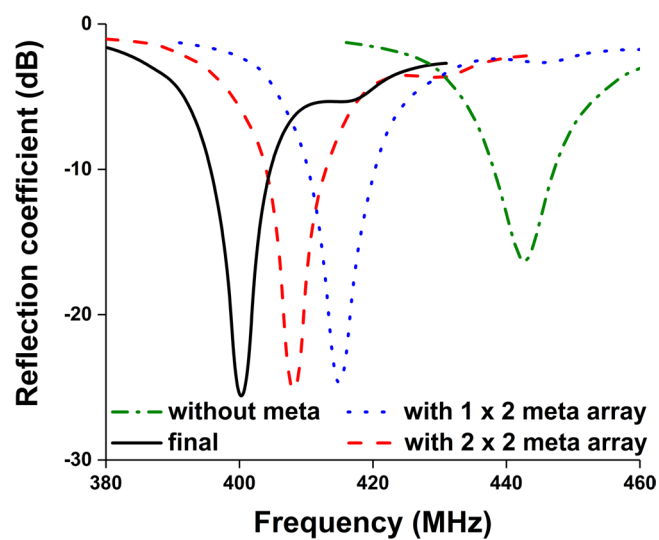


Figure 3. Investigation on reflection coefficient at the different design stages.

Parameter	Value (mm)	Parameter	Value (mm)
L	80	l	22.00
L_1	39.12	a	10.00
L_2	8.6	b	9.50
L_3	7.5	c	4.50
L_4	24	d	3.75
L_f	10.4	e	5.25
W	45	f	3.00
W_1	1.78	g_1	0.25
W_2	2.72	g_2	0.50
h	1.575	g_3	0.75
g	0.75		

Table 1. Optimized antenna design parameter.

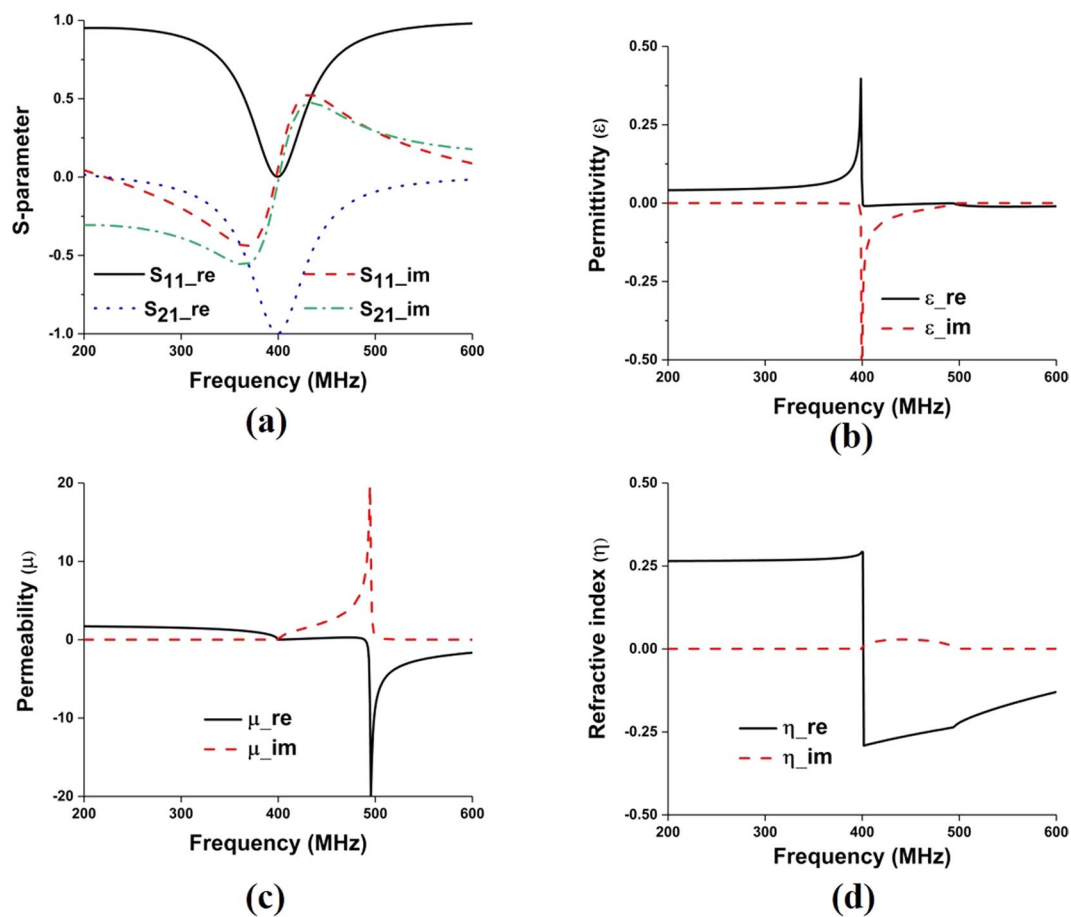


Figure 4. (a) Metamaterial reflection and transmission coefficient for single unit cell; and retrieved metamaterial characteristics- (b) permittivity, (c) permeability and (d) refractive index.

antenna. The performance of the proposed antenna has been characterized using CST microwave studio software and the prototype meander line antenna has been fabricated on Rogers 5800 dielectric, which has a thickness of 1.575 mm, a relative permittivity of 2.2, and loss tangent of 0.0013. The antenna geometry is depicted in Fig. 1. The initial antenna considered partial ground plane-based meander line to achieve lower UHF frequency resonator. However, the partial ground plane has a direct effect on complex circuit and structure. The resonant frequency might shift and also reduce the efficiency while the antenna placed in a close proximity to the metallic structure^{24,25}. To reduce this effect EMNZ metamaterial structure has been placed in the ground plane of the antenna. The array configuration of the metamaterial unit cell has been optimized until the desired antenna reflection coefficient and efficiency has been achieved. Moreover, the antenna has an omnidirectional radiation pattern, which has also been accomplished by the defected ground structure of EMNZ metamaterial array. The evolution stages are illustrated in Fig. 2, and the corresponding reflection coefficient is presented in Fig. 3. Figure 3 demonstrates

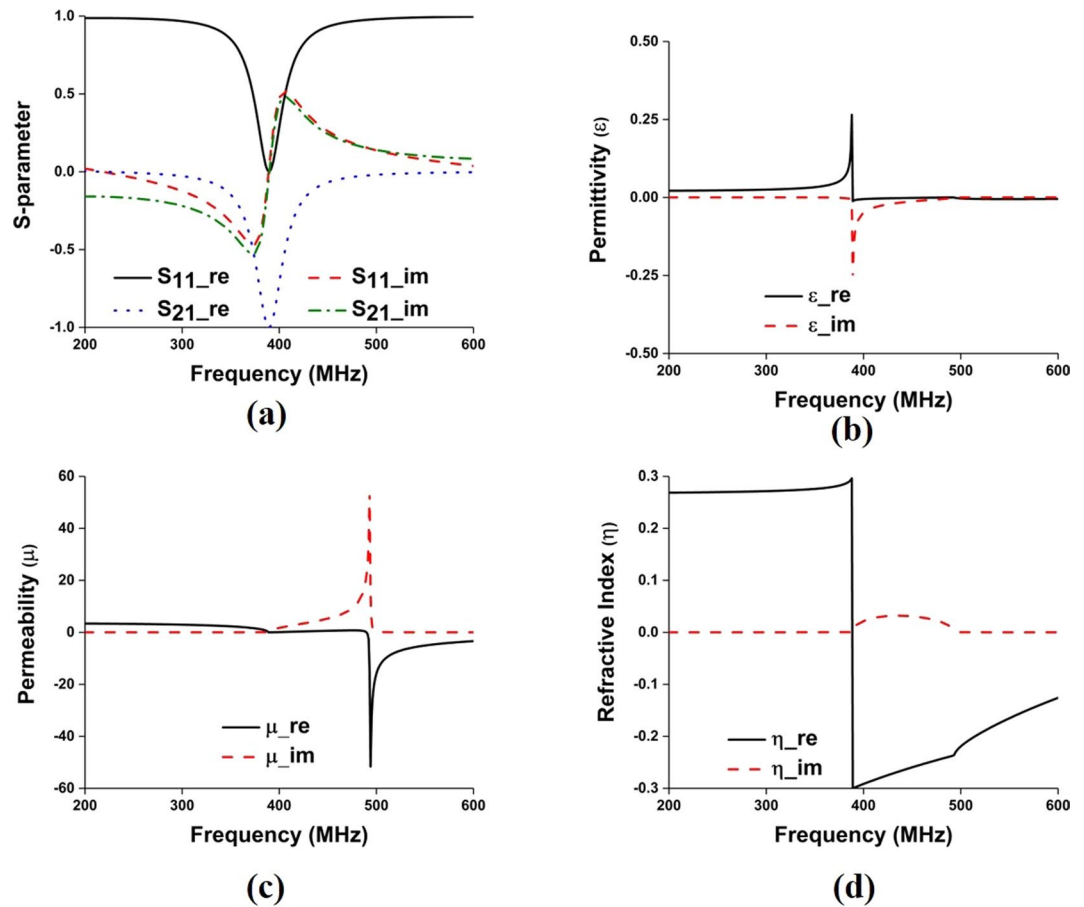


Figure 5. (a) Metamaterial reflection and transmission coefficient for 1×2 -unit cell array; and retrieved metamaterial characteristics- (b) permittivity, (c) permeability and (d) refractive index for 1×2 -unit cell array.

that the operating frequency of the antenna has been tuned at 401 MHz and observed the corresponding reflection coefficient. The proposed antenna has been optimized for 401 MHz operating frequency with 80% total radiation efficiency and the optimized design parameters are listed in Table 1.

EMNZ Metamaterial characterization

The proposed metamaterial is composed of thin metallic arms and split resonant rings (SRRs). The outer metallic arms are utilized to realize electric resonance and effective ϵ -near-zero (ENZ), and the interconnected split ring resonators are used to realize magnetic resonance and effective μ -near-zero (MNZ), so the designed structure shows the properties of an impedance-matched near-zero-index metamaterial with ENZ and MNZ simultaneously. The metamaterial structure has been designed and simulated using CST Microwave Studio. Perfect electric conductor (PEC) and perfect magnetic conductor (PMC) boundary conditions are used along X and Y axis, respectively and two waveguide ports have been assigned in Z-direction according to^{26,27}. The electromagnetic parameters of the proposed metamaterial have been retrieved using the following equations (1–9) of robust metamaterial parameter extraction method^{27,28}. In Fig. 4, the metamaterial parameters for the unit cell are depicted, where it can be observed that the proposed structure shows permittivity, permeability and refractive index value of -0.005 , 0.009 , and -0.007 , respectively. The metamaterials constitutive parameters show near-zero permittivity (ENZ), near-zero permeability (MNZ), and near-zero refractive index. Moreover, the metamaterial performance has been investigated for unit cell, 1×2 , 2×2 , and 3×2 array configuration using unit cell simulation setup, where 1×2 -unit cell array, 2×2 -unit cell array and 3×2 -unit cell array configuration shows EMNZ metamaterial characteristics, depicted in Figs 5–7, respectively. The summary of the study is listed in Tables 2 and 3.

$$S_{11} = \frac{R_{01}(1 - e^{i2nk_0d})}{1 - R_{01}^2 e^{i2nk_0d}} \quad (1)$$

$$S_{21} = \frac{(1 - R_{01}^2)e^{ink_0d}}{1 - R_{01}^2 e^{i2nk_0d}} \quad (2)$$

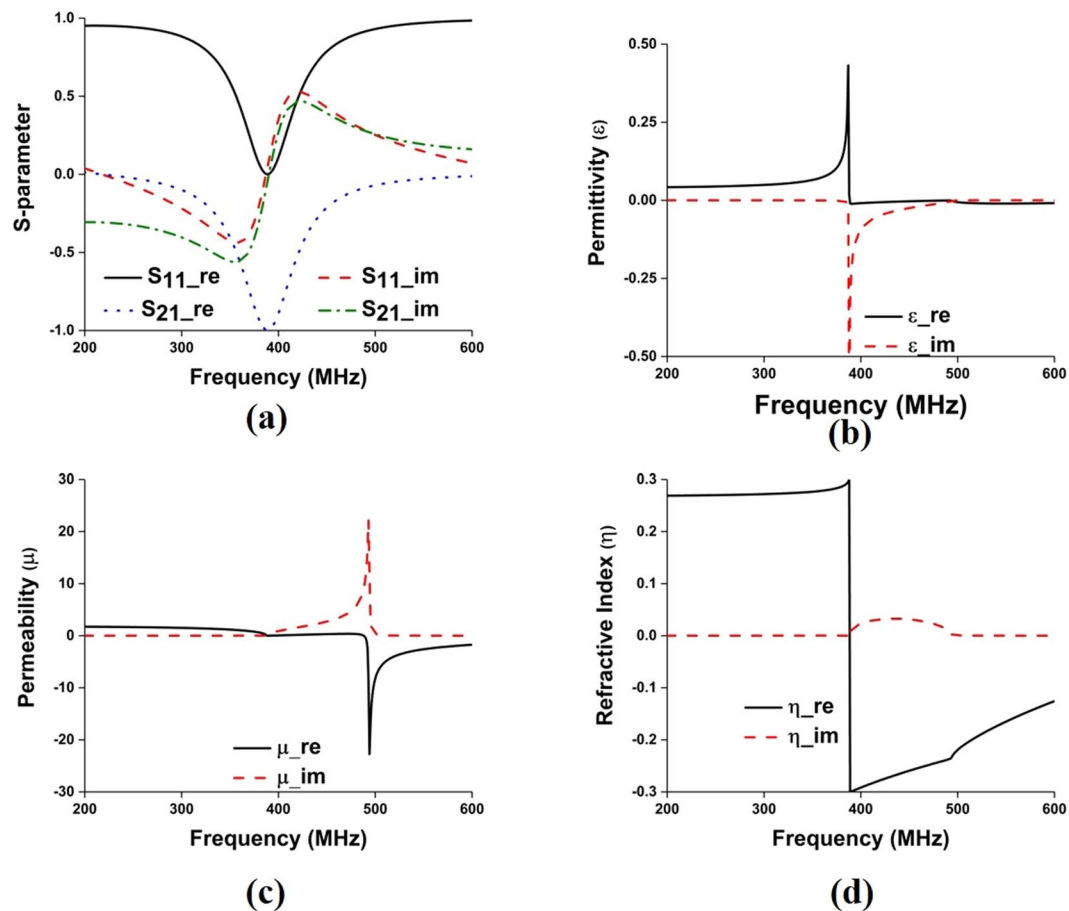


Figure 6. (a) Metamaterial reflection and transmission coefficient for 2×2 -unit cell array; and retrieved metamaterial characteristics- (b) permittivity, (c) permeability and (d) refractive index for 2×2 -unit cell array.

$$R_{01} = \frac{z - 1}{z + 1} \tag{3}$$

$$z = \pm \sqrt{\frac{(1 + S_{11})^2 + S_{21}^2}{(1 - S_{11})^2 + S_{21}^2}} \tag{4}$$

$$X = \frac{1}{2S_{21}(1 - S_{11}^2 + S_{21}^2)} \tag{5}$$

$$e^{ink_0d} = X \pm i\sqrt{1 - X^2} \tag{6}$$

$$\eta = \frac{1}{k_0d} \{ [\ln(e^{ink_0d})]'' + 2m\pi \} - i[\ln(e^{ink_0d})]' \} \tag{7}$$

$$\epsilon = \frac{\eta}{z} \tag{8}$$

$$\mu = \eta z \tag{9}$$

Antenna Performance Analysis

The antenna has been fabricated according to the optimized parameters listed in Table 1, illustrated in Fig. 8. A 50 Ohm micro-miniature coaxial (MMCX) connector is connected to feed the antenna. The connector height is 4.5 mm from the ground plane and diameter is 2.54 mm, which is compatible with small ground plane and nanosatellite structure. The reflection coefficient of the proposed antenna has been measured using performance

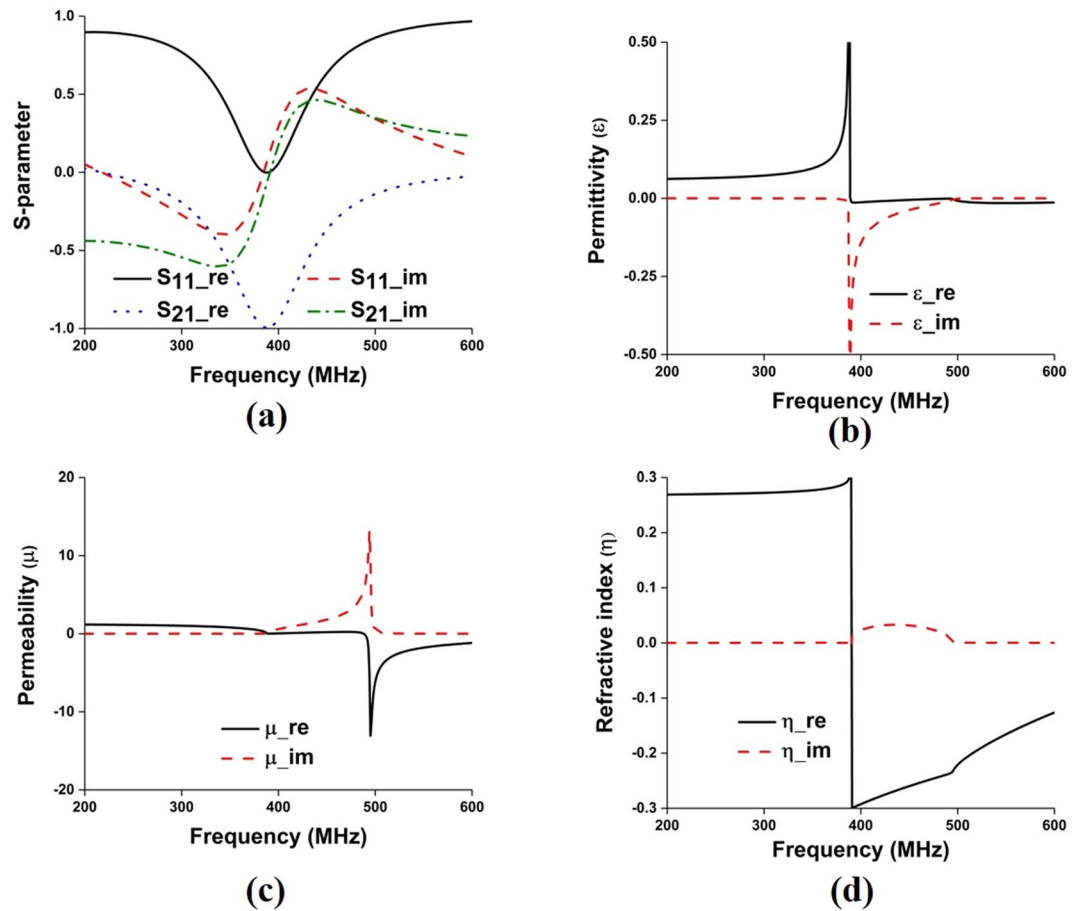


Figure 7. (a) Metamaterial reflection and transmission coefficient for 3×2 -unit cell array; and retrieved metamaterial characteristics- (b) permittivity, (c) permeability and (d) refractive index for 3×2 -unit cell array.

Configuration	Parameter	EMNZ index frequency region (MHz)
Unit Cell	Permeability, μ	200–600
	Permittivity, ϵ	397–493
	Refractive index, n	200–600
1×2 -unit cell array	Permeability, μ	2000–600
	Permittivity, ϵ	390–462
	Refractive index, n	200–600
2×2 -unit cell array	Permeability, μ	200–600
	Permittivity, ϵ	389–490
	Refractive index, n	200–600
3×2 -unit cell array	Permeability, μ	200–600
	Permittivity, ϵ	380–493
	Refractive index, n	200–600

Table 2. EMNZ frequency region of the retrieved effective parameters.

Configuration	Permittivity	Permeability	Refractive index
Unit Cell	−0.005	0.009	−0.007
1×2 -unit cell array	−0.005	0.07	−0.29
2×2 -unit cell array	−0.009	0.0542	−0.291
3×2 -unit cell array	−0.013	0.039	−0.293

Table 3. EMNZ properties of the proposed metamaterial at 401 MHz.

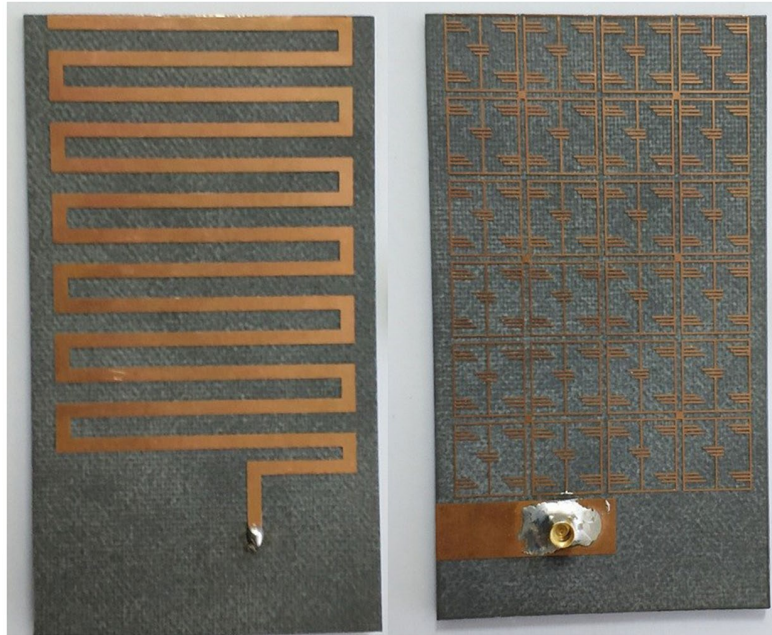


Figure 8. Fabricated prototype of the optimized metamaterial antenna.

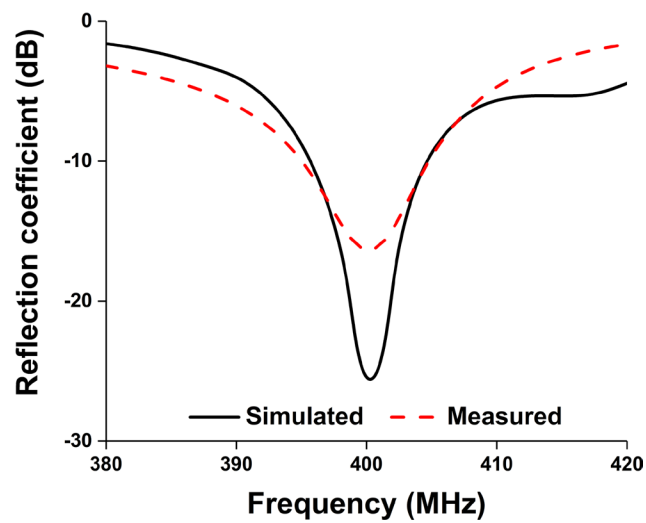


Figure 9. Simulated and measured reflection coefficient.

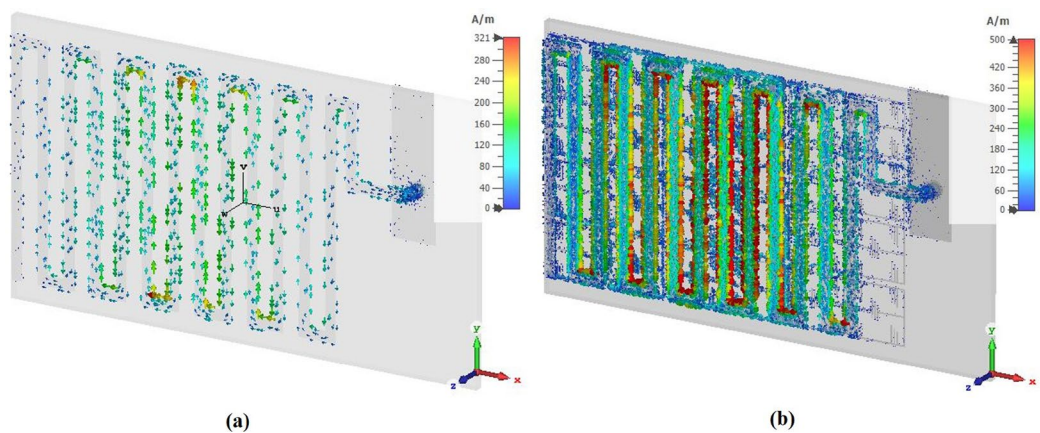


Figure 10. Surface current distribution at 401 MHz- (a) without metamaterial and (b) with metamaterial.

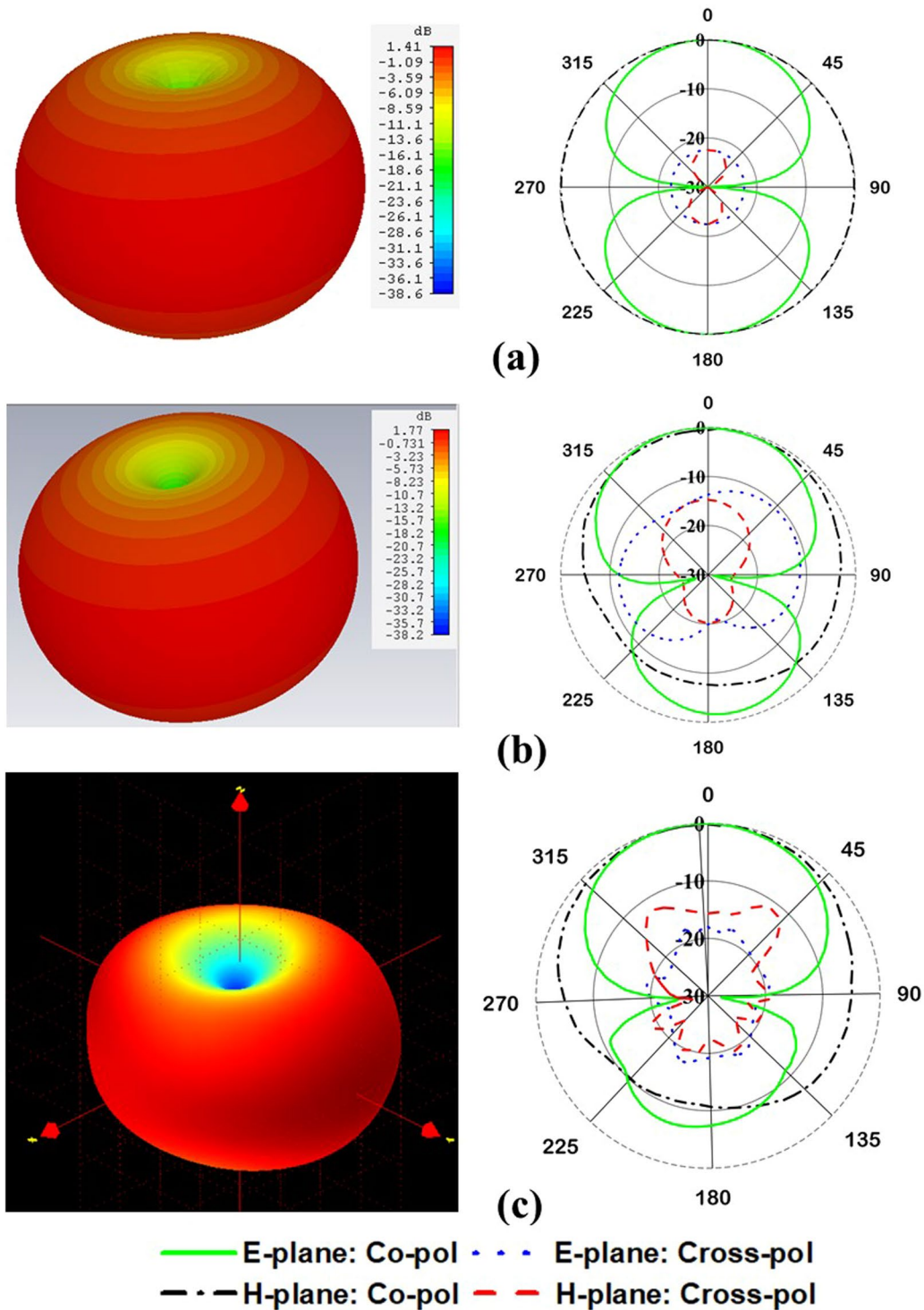


Figure 11. Radiation pattern at 401 MHz- (a) simulated pattern without metamaterial. (b) Simulated pattern with metamaterial and (c) measured pattern with metamaterial.

network analyzer (N5227A) that was calibrated using Electronic Calibration Module (N4694-60001). The simulated and measured reflection coefficient of the antenna has been analyzed, shown in Fig. 9. The proposed antenna has achieved -10 dB impedance bandwidth of 14.92 MHz (391 MHz–405.92 MHz).

The surface current of the antenna without and with metamaterial has been investigated, shown in Fig. 10. It is seen that a strong current is observed in meander line of the metamaterial antenna than without metamaterial antenna. It is predicted that the EMNZ structure has driven the surface current and act as strong radiation elements. Hence, the meander line with metamaterial radiated stronger radiation fields than without metamaterial antenna and contribute to improve the radiation efficiency and gain of antenna.

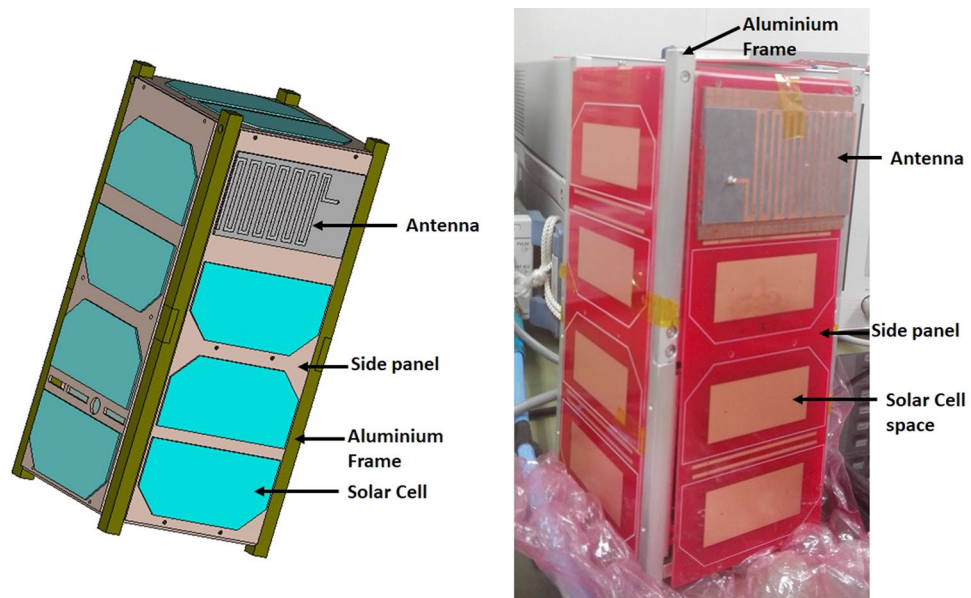


Figure 12. Antenna attachment with 2U nanosatellite structure- (a) simulation and (b) fabricated.

The antenna far-field characteristics have been investigated using Satimo near-field measurement system. The simulated and measured radiation patterns at 401 MHz with and without metamaterial are presented in Fig. 11. As it is expected, the antenna has approximately a dipole-like radiation pattern for conventional meander line antenna, Fig. 11(a) and realized gain of 1.44 dB is observed at 401 MHz. Moreover, when the EMNZ array structure placed at the antenna relatively strong current distributions are seen on the meandered line. Thus, stronger radiation is observed in boresight direction and the radiation pattern shifted from conventional one. In addition, the antenna shows simulated realized gain of 1.77 dB and measured the gain of 1.65 dB. Both simulated and measured radiation patterns are in good agreement.

Antenna performance with Nanosatellite Structure. The antenna has been integrated with 2U nanosatellite structure, illustrated in Fig. 12. The 2U nanosatellite structure was designed according to the Japan Aerospace Exploration Agency (JAXA) standard. The structure was considered as 227 +/- 0.1 mm tall (+Z axis), 100 +/- 0.1 mm wide (+X, +Y axes) and maximum weight was 2.6 Kg. Aluminium 7075 material was considered for the nanosatellite frame structure. The solar panels are connected with the back-plane board of the structure, which is FR-4 substrate material. The antenna has been mounted on the backplane using RTV glue (Room-Temperature-Vulcanizing glue). The UHF antenna performance has been investigated with nanosatellite structure for both antenna 1 (without EMNZ) and antenna 4 (proposed). The antennas have been tuned at 401 MHz with 2U nanosatellite structure, illustrated in Fig. 13. The corresponding total efficiency of 45% and 57.7% has been realized for without EMNZ and with EMNZ structure, respectively. It is interesting to observe that the antenna total efficiency with 2U nanosatellite structure is improved by 12.7% after integrating EMNZ metamaterial structures.

In addition, the radiation pattern of the antenna with the nanosatellite structure has been investigated for both 'with and without metamaterial' antenna, shown in Fig. 14. Both the radiation patterns are perturbed by nanosatellite structure and increased cross-polarization label with respect to free space condition. Compared with metamaterial-less (without metamaterial) antenna, the pattern is more spherical and provide more coverage of area of interest. Moreover, the realized gain obtained by without and with metamaterial antenna is 0.505 and 1.15 dB, respectively.

Moreover, the measured and simulated reflection coefficient bandwidth of the proposed antenna with 2U nanosatellite structure is 15 MHz (391–406 MHz) and 25 MHz (388–413.5 MHz), respectively. It is seen from Fig. 15 that both results agree reasonably well, except little frequency shifting issue. Though both results ensure operating frequency, the resonant frequency discrepancy is acceptable considering fabrication and assembly tolerance. A summary of the antennas mounted on nanosatellite structure is tabulated in Table 4.

Antenna Signal Propagation Test. The Free Space Path Loss (FSPL) using variable attenuation has been conducted to estimate the maximum signal propagation of the proposed antenna with active nanosatellite. The FSPL has been calculated considering LEO orbit nanosatellite (400 km). The free space path loss has been calculated using the Friis transmission equation²⁹ and represented in equation (10).

$$FSPL = 20 \log_{10}(d) + 20 \log_{10}(f) + 20 \log_{10}\left(\frac{4\pi}{c}\right) - G_{Tx} - G_{Rx} \quad (10)$$

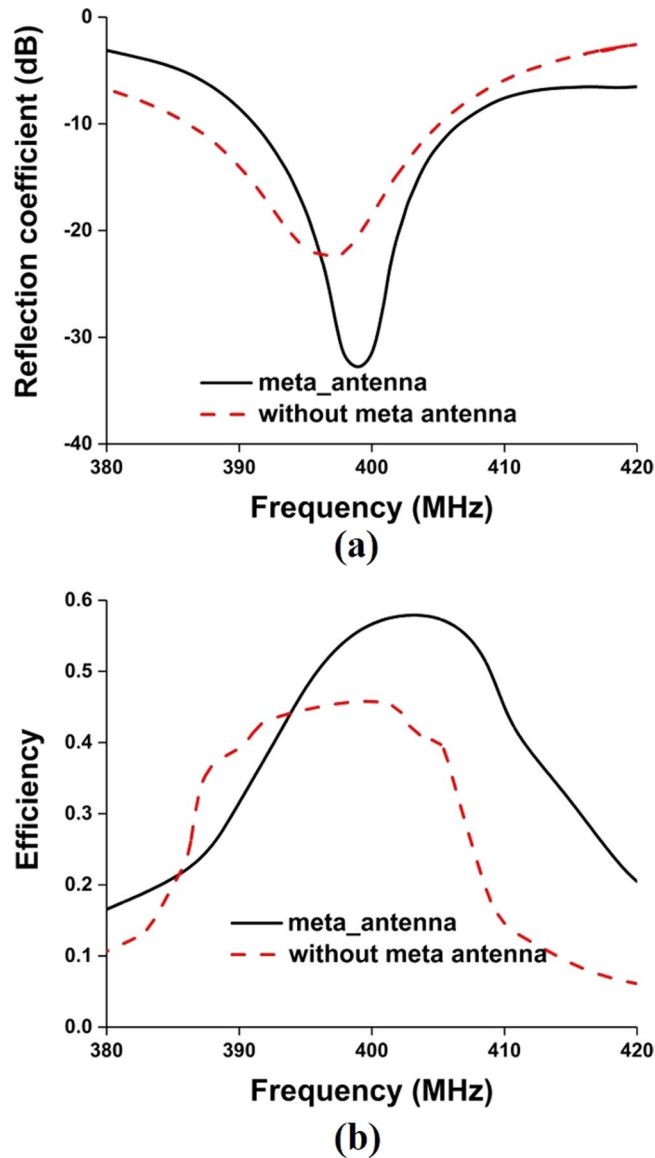


Figure 13. Antenna performance with nanosatellite structure- (a) reflection coefficient and (b) total efficiency.

Where d is the distance between receiver and transmitter end, f is the operating frequency, G_{Tx} is the transmitter antenna gain and G_{Rx} is receiver antenna gain.

The FSPL analysis using the proposed antenna is illustrated in Fig. 16(a). The signal modulation system is shown in Fig. 16(b). The active satellite with communication board has been placed on the anechoic chamber's turntable and proposed antenna (Tx) is transmitting signal. The receiving antenna (Rx) is positioned in the Horizontal orientation and connected to the Receiver through a variable attenuator. Attenuation increased gradually until the demodulation of the transmitted signal is no longer possible. The maximum attenuation value at which the receiver can demodulate the signal represents the signal strength of the transmitter antenna, which can address the maximum path loss. The SS power has been calculated by integrating over 100 kHz bandwidth. Care was taken to ensure that the RF power at receiver input never exceeds over -30 dBm and RF power received by the demodulator doesn't exceed over -50 dBm for extended time period to protect the devices.

$$\text{Gain of the proposed antenna at 401 MHz } (G_{Tx}) = 1.65 \text{ dBi}$$

$$\text{Gain of receiving antenna in anechoic chamber at 401 MHz } (G_{Rx}) = 6.9 \text{ dBi}$$

$$\text{Ground station antenna gain at 401 MHz } (G'_{Rx}) = 18 \text{ dBi}$$

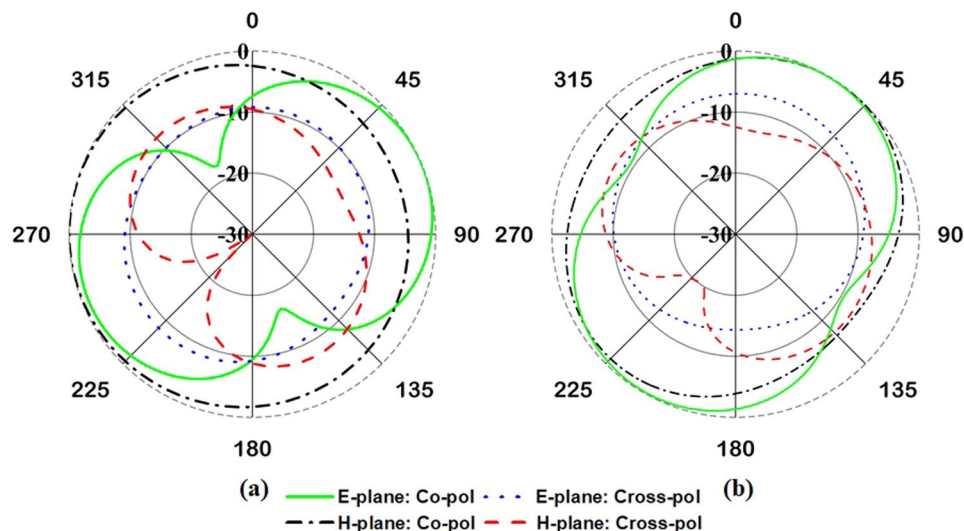


Figure 14. Normalized radiation pattern of the proposed antenna with nanosatellite structure- (a) without metamaterial and (b) with metamaterial.

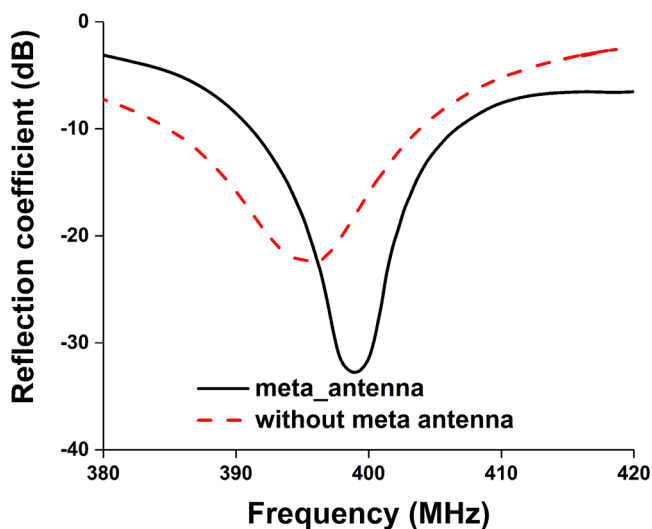


Figure 15. Measured and simulated reflection coefficient of the proposed antenna with nanosatellite structure.

Antenna performance	Without metamaterial	With metamaterial
Operating frequency (MHz)	386–404.5	391 MHz–405.92
Realized gain (dB)	0.505	1.15
Efficiency (%)	45	57.7
Frequency shift with different structures (MHz)	25–35	3–5

Table 4. A summary of the antennas mounted on nanosatellite structure.

Free Space Path loss (FSPL) in the chamber (360 cm) at 401 MHz = 27.1 dB

FSPL at orbital altitude (400 km) at 401 MHz = 116.8 dB

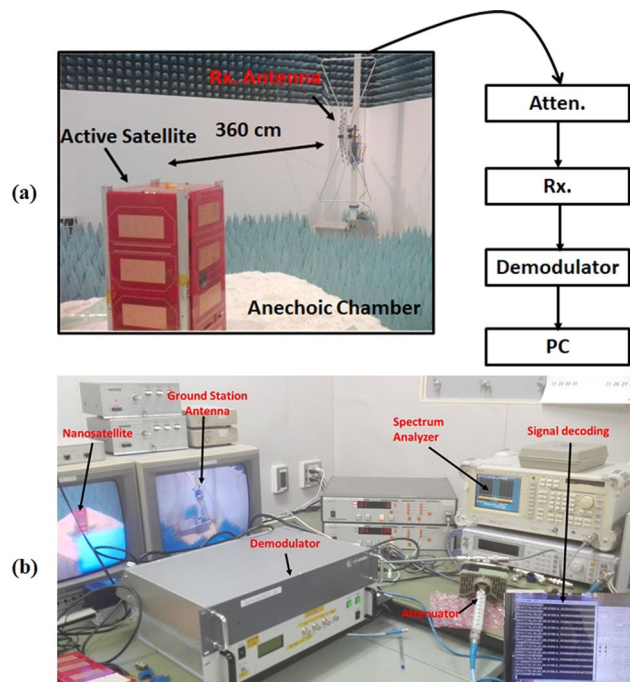


Figure 16. FSPL performance investigation of the nanosatellite using proposed antenna, (a) measurement layout and (b) Signal demodulation.

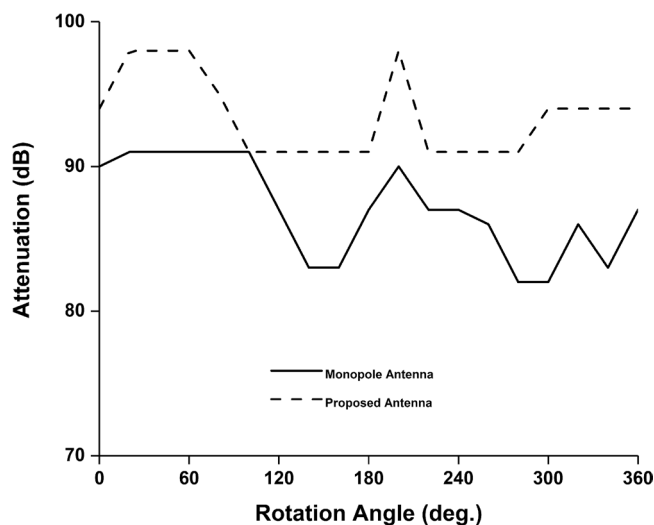


Figure 17. Maximum FSPL analysis using the proposed antenna and wire monopole antenna.

$$\begin{aligned}
 &\text{Extra attenuation required to achieve signal level estimation} \\
 &= \text{Orbital FSPL} - \text{FSPL(Chamber)} - G'_{\text{Rx}} + G_{\text{Rx}} \\
 &= 116.8 - 27.1 - 18 + 6.9 \\
 &= 78.6 \text{ dB}
 \end{aligned}$$

The attenuation level of the proposed antenna has been compared with conventional wire monopole antenna. From Fig. 17, it is shown that the proposed antenna signal transmission capability is higher than wire monopole antenna. The receiver can demodulate the transmitting signal up to maximum attenuation of 98 dB.

Reference	Antenna type & Size (mm)	Operating band (MHz)	Realized gain (dB)	Remarks
Liu <i>et al.</i> ³²	Printed patch 320 × 80 × 3.17	427.38–437.17	2.12	incompatible with 1U and 2U structure due to larger antenna size
Kakoyiannis <i>et al.</i> ³³	Microstrip patch 170 × 120 × 6.4	435–437	0.7	incompatible with 1U and 2U structure due to larger antenna size
Podilchak <i>et al.</i> ³⁴	Microstrip Patch 150 × 150 × 37	384–410	0.4	incompatible with 1U and 2U structure due to larger antenna size
Costantine <i>et al.</i> ³⁵	Deployable helix Helix heigh:500	365	8	High performance antenna but not compatible with 1U structure
Alam <i>et al.</i> ³⁶	3D-type antenna	398 MHz – 405 MHz	1.18	compatible with 1U and 2U structure but have design complexity
BIRDS-I CubeSat antenna ^{31,37,38}	Printed patch 72 × 32 × 1.575	418–448	0.55	compatible with 1U and 2U structure but mission incomplete due to low efficiency and frequency shifting issue
Proposed antenna	Printed patch 80 × 45 × 1.575	391 MHz – 405.92	1.77	compatible with 1U and 2U structure Free from deployable complexity

Table 5. A comparison of the presented antenna with different UHF nanosatellite antennas.

Discussion

The contributions of the proposed antenna are highlighted in this section. A comparison of the proposed antenna with some existing UHF nanosatellite antennas is presented in Table 5.

Deployment complexity free. RF failures in nanosatellite antenna have been reported by several incidents that have been occurred due to unsuccessful antenna deployment^{6,30}. The established deployment mechanism is burn-wire method, but it is quite sophisticated to test in laboratory environment. The proposed patch antenna with compact size of $45 \times 80 \times 1.575 \text{ mm}^3$ can mitigate this issue.

Enhanced patch Antenna performance. The proposed antenna holds the potential for smooth communication between nanosatellite and the Earth, as it provides substantially higher gain and efficiency with only $45 \times 80 \text{ mm}^2$ antenna dimension. The antenna addresses the frequency shifting issue that happens frequently in nanosatellite patch antenna and makes the mission risky³¹.

Ensure smooth communication. This research also emphasised on the nanosatellite communication test using the antenna that proves the validity of the antenna's real-time performance. The satellite ground station receiver can demodulate the transmitting signal up to maximum attenuation of 98 dB, which is 20 dB higher than required marginal Free Space Path Loss (FSPL). Moreover, the lab prototype of the antenna has undergone a vibration test while embedded with nanosatellite structure that proves the robustness of the antenna.

Conclusion

In this paper, an EMNZ metamaterial has been developed and integrated on the conventional meander line antenna ground plane to reduce the coupling effect with external auxiliary elements. The computational analysis of EMNZ metamaterial properties has been investigated for both unit cell and array configurations. The studies indicate that, compared with the conventional antenna, the proposed EMNZ structure has extended the antenna total efficiency by 12% without shifting resonant frequency. The free space path loss analysis has been performed to verify the feasibility of the proposed antenna for nanosatellite communication system.

References

- Heidt, H., Puig-Suari, J., Moore, A., Nakasuka, S. & Twigg, R. *CubeSat: A new generation of picosatellite for education and industry low-cost space experimentation*. (Logan, USA, 2000).
- Gao, S. *et al.* Antennas for modern small satellites. *IEEE Antennas and Propagation Magazine* **51** (2009).
- Rahmat-Samii, Y., Manohar, V. & Kovitz, J. M. For Satellites, Think Small, Dream Big: A review of recent antenna developments for CubeSats. *IEEE Antennas and Propagation Magazine* **59**, 22–30 (2017).
- Ernest, A. J., Tawk, Y., Costantine, J. & Christodoulou, C. G. A bottom fed deployable conical log spiral antenna design for CubeSat. *IEEE Transactions on Antennas and Propagation* **63**, 41–47 (2015).
- Atcitty, S. *AIHEC/TCU Advanced Manufacturing Network Initiative*. (Sandia National Lab.(SNL-NM), Albuquerque, NM (United States), 2016).
- Venturini, C., Braun, B., Hinkley, D. & Berg, G. Improving mission success of CubeSats. *Aerospace Corp., El Segundo, CA, USA, Aerospace Report No. TOR-2017-01689* (2017).
- Fernandes, G., Santos, M., Silva, V., Almeida, J. & Nogueira, P. Thermal tests for cubesat in Brazil: Lessons learned and the challenges for the future. In *Proceedings of the 67th International Astronautical Congress, Guadalajara* (Vol. 27) (Mexico, September, 2016).
- Sarabandi, K., Buerkle, A. M. & Mosallaei, H. Compact wideband UHF patch antenna on a reactive impedance substrate. *IEEE antennas and wireless propagation letters* **5**, 503 (2006).
- Wu, J. & Sarabandi, K. Reactive impedance surface TM mode slow wave for patch antenna miniaturization [AMTA corner]. *IEEE Antennas and Propagation Magazine* **56**, 279–293 (2014).
- Rashed, J. & Tai, C.-T. A new class of resonant antennas. *IEEE Transactions on Antennas and Propagation* **39**, 1428–1430 (1991).
- Landy, N. I., Sajuyigbe, S., Mock, J., Smith, D. & Padilla, W. Perfect metamaterial absorber. *Physical review letters* **100**, 207402 (2008).
- Enoch, S., Tayeb, G., Sabouroux, P., Guérin, N. & Vincent, P. A metamaterial for directive emission. *Physical Review Letters* **89**, 213902 (2002).
- Zhang, K. *et al.* Phase-engineered metalenses to generate converging and non-diffractive vortex beam carrying orbital angular momentum in microwave region. *Optics express* **26**, 1351–1360 (2018).

14. Zhang, K., Ding, X., Wo, D., Meng, F. & Wu, Q. Experimental validation of ultra-thin metalenses for N-beam emissions based on transformation optics. *Applied Physics Letters* **108**, 053508 (2016).
15. Ullah, M. H. & Islam, M. T. A new metasurface reflective structure for simultaneous enhancement of antenna bandwidth and gain. *Smart materials and Structures* **23**, 085015 (2014).
16. Ratni, B., de Lustrac, A., Piau, G.-P. & Burokur, S. N. Electronic control of linear-to-circular polarization conversion using a reconfigurable metasurface. *Applied Physics Letters* **111**, 214101 (2017).
17. Ratni, B., de Lustrac, A., Piau, G.-P. & Burokur, S. N. Reconfigurable meta-mirror for wavefronts control: applications to microwave antennas. *Optics express* **26**, 2613–2624 (2018).
18. Mahmoud, A. M. & Engheta, N. Wave-matter interactions in epsilon-and-mu-near-zero structures. *Nature communications* **5**, 5638 (2014).
19. Dehbashi, R., Bialkowski, K. S. & Abbosh, A. M. Size Reduction of Electromagnetic Devices Using Double Near-Zero Materials. *IEEE Transactions on Antennas and Propagation* **65**, 7102–7109 (2017).
20. Liu, Y., Zhou, X., Zhu, Z. & Zhao, X. Broadband impedance-matched near-zero-index metamaterials for a wide scanning phased array antenna design. *Journal of Physics D: Applied Physics* **49**, 075107 (2016).
21. Soric, J. C., Engheta, N., Maci, S. & Alu, A. Omnidirectional Metamaterial Antennas Based on ϵ -Near-Zero Channel Matching. *IEEE Transactions on Antennas and Propagation* **61**, 33–44 (2013).
22. Yang, J. J., Francescato, Y., Maier, S. A., Mao, F. & Huang, M. Mu and epsilon near zero metamaterials for perfect coherence and new antenna designs. *Optics express* **22**, 9107–9114 (2014).
23. Ullah, M. H. *et al.* ZIM cover for improvement of the bandwidth and gain of patch antenna. *Current Applied Physics* **16**, 837–842 (2016).
24. Qing, X. & Chen, Z. N. Proximity effects of metallic environments on high frequency RFID reader antenna: Study and applications. *IEEE transactions on Antennas and Propagation* **55**, 3105–3111 (2007).
25. Ukkonen, L., Sydanheimo, L. & Kivikoski, M. Effects of metallic plate size on the performance of microstrip patch-type tag antennas for passive RFID. *IEEE Antennas and Wireless Propagation Letters* **4**, 410–413 (2005).
26. Zarghooni, B., Dadgarpour, A. & Denidni, T. A. Greek-key pattern as a miniaturized multiband metamaterial unit-cell. *IEEE Antennas and Wirel. Propag. Lett* **14**, 1254–1257 (2015).
27. Islam, M. T., Bin Ashraf, F., Alam, T., Misran, N. & Singh, M. S. J. Investigation of Left-Handed Meta-Atom for Radio Frequency Shielding Application. *Science of Advanced Materials* **10**, 1582–1587 (2018).
28. Chen, X., Grzegorzczak, T. M., Wu, B.-I., Pacheco, J. Jr. & Kong, J. A. Robust method to retrieve the constitutive effective parameters of metamaterials. *Physical review E* **70**, 016608 (2004).
29. Saakian, A. *Radio wave propagation fundamentals*. (Artech House, 2011).
30. Saunders, A. A Failure Analysis of the EXOCUBE CubeSat, *13th Annual Cubesat Workshop*, San Luis Obispo, USA, 20-04-2016.
31. Samsuzzaman, M., Islam, M. T., Kibria, S. & Cho, M. BIRDS-1 CubeSat Constellation Using Compact UHF Patch Antenna. *IEEE Access* **6**, 54282–54294 (2018).
32. Liu, X. *et al.* Transparent and Nontransparent Microstrip Antennas on a CubeSat: Novel low-profile antennas for CubeSats improve mission reliability. *IEEE Antennas and Propagation Magazine* **59**, 59–68 (2017).
33. Kakoyiannis, C. G. & Constantinou, P. A compact microstrip antenna with tapered peripheral slits for CubeSat RF Payloads at 436 MHz: Miniaturization techniques, design & numerical results, *IEEE International Workshop on Satellite and Space Communications (IWSSC)*, 255–259 (2008).
34. Podilchak, S. K., Murdoch, A. P. & Antar, Y. M. Compact, Microstrip-Based Folded-Shorted Patches: PCB antennas for use on microsatellites. *IEEE Antennas and Propagation Magazine* **59**, 88–95 (2017).
35. Costantine, J. *et al.* UHF deployable helical antennas for CubeSats. *IEEE Transactions on Antennas and Propagation* **64**, 3752–3759 (2016).
36. Alam, T. *et al.* Design and compatibility analysis of a solar panel integrated UHF antenna for nanosatellite space mission. *PLoS one* **13**, e0205587 (2018).
37. Basyirah, S. BIRDS-2 Antenna Selection Design & Configuration. *BIRDS Project Newsletter*, 25–29 (2017).
38. *Nanosatellite & CubeSat Database* [Missions, constellations, <https://www.nanosats.eu/>] (2019).

Acknowledgements

This research is a collaboration work between Universiti Kebangsaan Malaysia and the Laboratory of Spacecraft Environment Interaction Engineering (LaSEINE), Kyushu Institute of Technology, Japan. This work is supported by the research university grant of Universiti Kebangsaan Malaysia.

Author Contributions

The antenna design and analysis were performed by Touhidul Alam. Prototype fabrication, characterization experiment and antenna performance characterization were conducted by Touhidul Alam, and Mohammad Tariqul Islam. The experimental set-up for nanosatellite structure was established by Mengü Cho. The project was supervised by Mohammad Tariqul Islam.

Additional Information

Supplementary information accompanies this paper at <https://doi.org/10.1038/s41598-019-40207-3>.

Competing Interests: The authors declare no competing interests.

Publisher's note: Springer Nature remains neutral with regard to jurisdictional claims in published maps and institutional affiliations.



Open Access This article is licensed under a Creative Commons Attribution 4.0 International License, which permits use, sharing, adaptation, distribution and reproduction in any medium or format, as long as you give appropriate credit to the original author(s) and the source, provide a link to the Creative Commons license, and indicate if changes were made. The images or other third party material in this article are included in the article's Creative Commons license, unless indicated otherwise in a credit line to the material. If material is not included in the article's Creative Commons license and your intended use is not permitted by statutory regulation or exceeds the permitted use, you will need to obtain permission directly from the copyright holder. To view a copy of this license, visit <http://creativecommons.org/licenses/by/4.0/>.

© The Author(s) 2019